A Journal of the Gesellschaft Deutscher Chemiker

Angewandte International Edition GDCh Chemie

www.angewandte.org

Accepted Article

Title: Redox Molecular Junction Metal-Covalent Organic Frameworks for Light-assisted CO2 Energy Storage

Authors: Jia-Nan Chang, Shan Li, Qi Li, Jian-Hui Wang, Can Guo, Yi-Rong Wang, Yifa Chen, Shun-Li Li, and Ya-Qian Lan

To be cited as: *Angew. Chem. Int. Ed.* **2024**, e202402458

Link to VoR: https://doi.org/10.1002/anie.202402458

WILEY VCH

10.1002/anie.202402458

WILEY-VCH

RESEARCH ARTICLE

Redox Molecular Junction Metal-Covalent Organic Frameworks for Light-assisted CO_2 Energy Storage

Jia-Nan Chang[a, b], Shan Li [b], Qi Li[a], Jian-Hui Wang[b], Can Guo[a], Yi-Rong Wang[a], Yifa Chen[a]*, Shun-Li Li[a], Ya-Qian Lan[a]*

[a] Dr. J.-N. C., Q. L., C. G., Y.-R. W., Prof. Y. C., Prof. S.-L. L. and Prof. Y.-Q. L.
School of Chemistry, South China Normal University, Guangzhou, 510006, P. R. China
[b] Dr. S., L., J.-H. W.
Jiangsu Collaborative Innovation Centre of Biomedical Functional Materials, Jiangsu Key Laboratory of New Power Batteries, School of Chemistry and Materials Science
Nanjing Normal University
Nanjing 210023, P. R. China
E-mail: chyf927821@163.com; E-mail: yqlan@m.scnu.edu.cn

Supporting information for this article is given via a link at the end of the document.

Abstract: Visible-light sensitive and bi-functionally favored CO_2 reduction (CRR)/evolution (CER) photocathode catalysts that can get rid of the utilization of ultraviolet light and improve sluggish kinetics is demanded to conquer the current technique-barrier of traditional Li-CO_2 battery. Here, a kind of redox molecular junction sp^2c metal-covalent organic framework (i.e. Cu_3-BTDE-COF) has been prepared through the connection between Cu_3 and BTDE and can serve as efficient photocathode catalyst in light-assisted Li-CO_2 battery. Cu_3-BTDE-COF with redox-ability, visible-light-adsorption region, electron-hole separation ability and endows the photocathode with excellent round-trip efficiency (95.2%) and an ultralow voltage hysteresis (0.18 V), outperforming the Schiff base COFs (i.e. Cu_3-BTDA-COF and Cu_3-DT-COF) and majority of the reported photocathode catalysts. Combined theoretical calculations with characterizations, Cu_3-BTDE-COF with the integration of Cu_3 centers, thiazole and cyano groups possess strong CO_2 adsorption/activation and Li^+ interaction/diffusion ability to boost the CRR/CER kinetics and related battery property.

Introduction

Nowadays, the energy consumption is still dominated by non-renewable fuels such as fossil fuels and the challenge of insufficient energy supply is becoming increasingly prominent, thus it is crucial to explore innovative and substitutable energy sources [1-4]. Aprotic Li-CO_2 battery based on the reversible electrochemical CO_2 reduction (CRR) and evolution (CER) reactions offers an CO_2 fixation approach as well as energy storage for diverse applications like power plant or Mars exploration [5-8]. Specially, it possesses a superior theoretical energy density (1876 Wh kg^{-1}) to Li-ion battery based on the reversible reaction: $4Li + 3CO_2 \rightleftharpoons 2Li_2CO_3 + C$ (E_0 = 2.80 V vs. Li^+/Li [5, 9-11]. To date, plenty of nanomaterials (e.g., noble metals, carbon materials and transition metal oxides) have been applied in Li-CO_2 batter [12-15]. However, there are some bottlenecks restrict its practical applications, such as high overpotential, poor round-trip efficiency or low-rate performance, etc., which mainly come from the slow charge/discharge reaction kinetic [16, 17]. In most of Li-CO_2 battery systems, the sluggish reaction kinetics especially that caused by the insulation or low decomposable properties of Li_2CO_3 during the discharge/charge processes lead to large voltage gap (mostly >1 V) and poor reversible ability [18, 19]. The difficulty in decomposing discharge products calls for advanced auxiliary technologies to overcome technical barriers of traditional Li-CO_2 battery, yet it remains a daunting challenge to achieve this goal [20, 21].

Light energy, an external driving force to promote the electrode reactions, has been highlighted as an attractive and alternative strategy for Li-CO_2 batter [22]. During the operation of light-assist Li-CO_2 battery, a certain amount of incident light can excite a large number of photo-generated electrons and holes on catalysts based on the photoelectric effect to promote the CRR and CER, thus reducing voltage hysteresis and improving battery efficiency [6, 22-24]. During the past years, only a few cathode catalysts such as In_2S_3@CNT/SS[23], CNT@C_3N_4[24], SiC@RGO[25], CoPc-Mn-O[6], or TiO_2/CC[26], have been investigated in light-assisted Li-CO_2 battery. However, they still face drawbacks like: i) the light absorption for most of the generally applied semiconductors are still in the ultraviolet region [26]; ii) the study of mechanisms for the light-assisted interaction are still rare and iii) most of materials are based on nonporous or hybrid materials, which are difficult to make full use of the active sites or precisely modulate their inherent structures [6, 23, 25]. Therefore, it is meaningful to specially develop photocatalysts with broad light absorption range, high porosity or well-designed functional groups to accelerate the reaction kinetics of CRR/CER to meet the demands of advanced light-assisted Li-CO_2 battery.

In this regard, covalent organic frameworks (COFs), a kind of crystalline porous polymers connected by strong covalent bond, come to our mind as a promising candidate for light-assisted Li-CO_2 battery [27-30]. Since 2005, COFs with the properties of pre-desirable structures/functions, high stability and porosity have attracted a lot of attention in various application fields like gas adsorption/separation, sensing, catalysis, drug delivery or energy storages, et [31, 32]. Among these advantages, the most remarkable one is their highly tunable and modifiable structures that can be accurately constructed through the selection of well-designed struts to meet the requirements of advanced applications like Li-CO_2 battery. Metal-covalent organic frameworks (MCOFs), a kind of interesting COFs obtained through the covalent bonding between metal clusters and organic ligands, possesses combined properties and advantages of both metal-organic frameworks (MOFs) and COFs, in which the metal clusters simulated from MOFs can serve as active sites while the covalent connection would be highly tolerant for many potentially

10.1002/anie.202402458

harsh application [33, 34]. Especially for the covalent connection obtained through low-reversible vinylene linkages, the resultant sp^2 carbon-conjugated COFs (sp^2c-COFs) might present high chemical stability, in-plane conjugations, functional -CN groups and porous frameworks that are much attractive for energy related applications [35-37]. Thus, if the functions of sp^2c-COF and MCOF can be well-combined, the generated sp^2c-MCOF might serve as very promising candidates to serve as ideal light-assisted Li-CO_2 photocathode catalysts due to the following advantages: i) COFs can be photo-absorbent by introducing photosensitive groups; ii) the adjustable structures would endow MCOFs with efficient ligand-metal charge transfer (LMCT) effect for enhanced electron-hole separation efficiency that might serve as redox molecular junction units for CRR and CER[38, 39]; iii) the carbon-carbon double bonds and additionally existed -CN groups in sp^2c-MCOF enhance the π conjugated electron transition, which might increase the electron mobility or Li^+ interaction[40-42] iv) MCOFs with ordered and well-defined structures are beneficial for mechanism study. Up to date, their applications in light-assisted Li-CO_2 battery remain an unexplored field and need much efforts to be made. Therefore, it is desirable to design and synthesize sp^2c-MCOF with multifunctional active sites to meet the requirements of CRR and CER for high performance light-assisted Li-CO_2 battery.

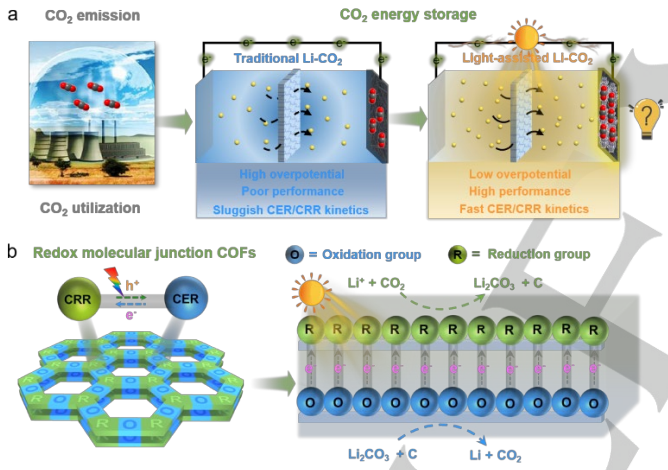

Scheme 1. Schematic representation of redox molecular junction COFs for light-assisted CO_2 energy storage. (a) The comparison of traditional Li-CO_2 battery and light-assisted Li-CO_2 battery. (b) The advantages of redox molecular junction COFs in light-assisted Li-CO_2 battery.

Herein, a kind of redox molecular junction sp^2c-MCOF (i.e. Cu_3-BTDE-COF) with multiple active sites are synthesized by in-situ covalent connection of Cu cluster (Cu_3), 2,2'-(benzo[c][1,2,5]thiadiazole-4,7-diylbis(4,1-phenylene))diacetonitrile (BTDE) that can serve as desired platform to be applied in light-assisted Li-CO_2 battery (Scheme 1). Specifically, the covalent connection between Cu_3 and BTDE in Cu_3-BTDE-COF enables the visible light driven electron-hole to efficiently separate and transfer from BTDE (oxidation group) to Cu_3 (reduction group) moiety, resulting in the photoexcited electrons on Cu_3 and holes on BTDE, respectively. Notably, Cu_3-BTDE-COF based cell offers an ultralow voltage hysteresis (0.18 V), outperforming Schiff base COFs (i. e. Cu_3-BTDA-COF and Cu_3-DT-COF), which is one of the best photocathode reported to date (Table S1 and S2). In addition, theoretical calculations and characterization have shown that Cu_3-BTDE-COF with the integration of metal active centers, thiazole and cyano multifunctional groups possesses strong CO_2 adsorption/activation and Li^+ interaction/diffusion ability, thereby improving overall battery efficiency.

Results and Discussion

Structural design and fabrication of photocatalysts. Cu_3-BTDE-COF has been synthesized by the condensation reaction of [Cu_3(PyCA)$_3$] (Cu_3) and 2,2'-(benzo[c][1,2,5]thiadiazole-4,7-diylbis(4,1-phenylene))diacetonitrile (BTDE) (detail see Methods). A kind of reddish-brown powder can be obtained after 72 h reaction at 150 °C and the structure of the sample is confirmed by the powder X-ray diffraction (PXRD) combined with structural simulation (Figure 1a and Figure S1). On the basis of theoretical structural simulation and Pawley refinements, the Cu_3-BTDE-COF can be fitted into the ABC stacking model with the corresponding unit cell parameters of a = 48.00 Å, b = 48.00 Å, and c = 2.63 Å, and α = β = 90°, γ = 120° in the R_3 space group (Table S3). As revealed by the differential plot, the refinement of PXRD pattern is well agreement with the experimental one (unweighted-profile R factor (R_p), 2.62% and weighted profile R factor (R_{wp}), 3.38%), suggesting the validity of the computational model (Figure 1c and e). In the PXRD pattern, it has intense peaks at 3.68°, 6.39°, 7.36°, and 10.13°, which can be ascribed to the (1 1 0), (3 0 0), (2 2 0) and (2 1 1) facets of Cu_3-BTDE-COF, respectively. In addition, Fourier transform infrared spectroscopy (FTIR) has been applied to characterize the chemical compositions of Cu_3-BTDE-COF. In the FTIR spectra, the stretching vibration at 1620 cm^{-1} can be attributed to the C=C in the resultant Cu_3-BTDE-COF, suggesting the successful formation of Cu_3-BTDE-COF. Meanwhile, this result can be further certified by the obviously decreased -CHO stretching vibration band (1699 cm^{-1}). Besides, the cyano group stretching vibration at 2220 cm^{-1} belongs to BTDE of Cu_3-BTDE-COF [43, 44].

In addition, X-ray photoelectron spectroscopy (XPS) analysis has been carried out to investigate the chemical states of the existed elements in Cu_3-BTDE-COF. For the XPS spectra of Cu_3-BTDE-COF, five main peaks with binding energy of 933.85, 164.65, 284.64, 399.10 and 531.55 eV are attributed to Cu 2p, S 2p, C 1s and O 1s, respectively (Figure S2). The C 1s spectra display two peaks with binding energy at 286.35 and 284.70 eV, respectively. The peak at 286.35 eV is assigned to the cyano group, and the peak at 284.70 eV belongs to the C-C/C=C bonds of the Cu_3-BTDE-COF [45]. In the Cu 2p region, peaks of 935.13 and 933.65 eV are assigned to Cu^{2+} and Cu^+, respectively, which complies previously reported works [46]. In detail, the appearance of Cu^{2+} is due to the surface oxidation, and the Cu valence can be switched between Cu^+ and Cu^{2+} without altering the components of Cu_3. In addition, the XPS spectra of S, C and O elements of Cu_3-BTDE-COF are shown in Figure S4. In the S 2p region, peaks at 164.07 eV (S $2p_{3/2}$) and 165.29 eV (S $2p_{1/2}$) can be attributed to the characteristic peaks of N-S bond in BT monomer (Figure S2). Besides, its N 1s spectra displays a single peak at 398.40 eV, corresponding to the C=N/C-N of Cu_3-BTDE-COF [47].

Additionally, Cu_3-BTDA-COF and Cu_3-DT-COF with 4,4'-(benzo-2,1,3-thiadiazole-4,7-diyl)dianiline (BTDA) and 4,4"-

10.1002/anie.202402458

WILEY-VCH

diamino-triphenyl (DT) substituted BTDE of Cu_3-BTDE-COF have also been synthesized as contrastive samples of Cu_3-BTDE-COF (Table S4 and S5). For Cu_3-BTDA-COF and Cu_3-DT-COF, their experimental PXRD patterns show high crystallinity, which are in good agreement with their simulated ones (Figure 1b and d). In addition, the compositions of them have also been characterized by FTIR and XPS tests (Figure S3-S8). It can be seen from the above test results that Cu_3-BTDA-COF and Cu_3-DT-COF have been successfully synthesized that can serve as ideal contrast samples to be compared with Cu_3-BTDE-COF.

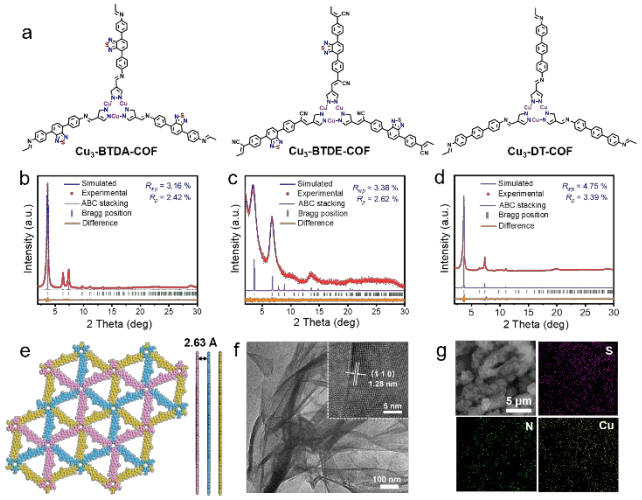

Figure 1. Structure and characterization of Cu_3-BTDE-COF, Cu_3-BTDA-COF and Cu_3-DT-COF. (a) Schematic representation of the syntheses of Cu_3-BT-COF, Cu_3-pT-COF and TFP-BT-COF. (b-d) Experimental (red dot) and simulated (blue line) PXRD patterns of Cu_3-BTDE-COF (c), Cu_3-BTDA-COF (b) and Cu_3-DT-COF (d). (e) Top and side views of the structure of Cu_3-BTDE-COF. (f) The HRTEM image and lattice fringes of Cu_3-BTDE-COF (insert is the circled place in f). (g) SEM and elemental mapping images of Cu_3-BTDE-COF.

The porosity of Cu_3-BTDE-COF has been evaluated by N_2 sorption tests at 77 K (Figure S9). The Brunauer-Emmett-Teller surface area (S_{BET}) of Cu_3-BTDE-COF is calculated to be 151 m^2 g^{-1}. To evaluate the CO_2 adsorption ability of Cu_3-BTDE-COF, the CO_2 adsorption test is carried out and it presents CO_2 uptake capacity of 33.7 cm^3 g^{-1} and 12.5 cm^3 g^{-1} at 273 K and 298 K, respectively (Figure S10). Moreover, the morphology of the synthesized Cu_3-BTDE-COF have been studied by transmission electron microscopy (TEM) and scanning electron microscope (SEM). Figure 1f shows the typical TEM image of Cu_3-BTDE-COF, demonstrating a layer-stacked morphology. Specifically, the oriented lattice fringes of Cu_3-BTDE-COF are clearly visible and the detected lattice spacing of 1.28 nm can be ascribed to the (1 1 0) plane in the high-resolution TEM (HR-TEM) image, proving the high crystallinity of Cu_3-BTDE-COF (Figure 1f). Besides, the elemental mapping analysis displays that Cu, N and S are homogenously distributed in Cu_3-BTDE-COF (Figure 1g). The above morphology characterizations further confirm that Cu_3-BTDE-COF has good crystallinity and long-range ordering structure. In addition, the morphology of Cu_3-BTDA-COF and Cu_3-DT-COF has also been characterized by SEM and TEM tests (Figure S11-S14).

Characterization of photocatalysts. In order to improve the electrochemical property, the photocathode for light-assisted Li-CO_2 battery needs to exhibit effective utilization of the light and low recombination rate for the photogenerated electron-hole pairs [48]. Therefore, the light absorption ability, electrons-holes separation efficiency and energy band structure of the sample have been analyzed. Initially, the optical absorption performances of Cu_3-BTDE-COF, Cu_3-BTDA-COF and Cu_3-DT-COF are carried out by ultraviolet and visible (UV-Vis) absorption spectra (Figure 2a). The band gaps (E_g) of Cu_3-BTDE-COF, Cu_3-BTDA-COF and Cu_3-DT-COF are determined to be 2.13, 2.01 and 2.69 eV by their Tauc plots, indicating that they all possess the properties of semiconductors (Figure S15) [6, 23]. In addition to these, Mott-Schottky measurements have also been performed to study the band positions of Cu_3-BTDE-COF, Cu_3-BTDA-COF and Cu_3-DT-COF (Figure 2c). The lowest unoccupied molecular orbital (LUMO) of the Cu_3-BTDE-COF is calculated to be 2.09 V versus Li^+/Li. Meanwhile, the highest occupied molecular orbital (HOMO) is calculated to be 3.89 V. As shown in Figure 2d, Cu_3-BTDE-COF fulfills the essential requirement of the light-assisted Li-CO_2 battery that the redox potential of CO_2/Li_2CO_3 (2.80 V vs Li^+/Li) is located between the LUMO and HOMO [49, 50].

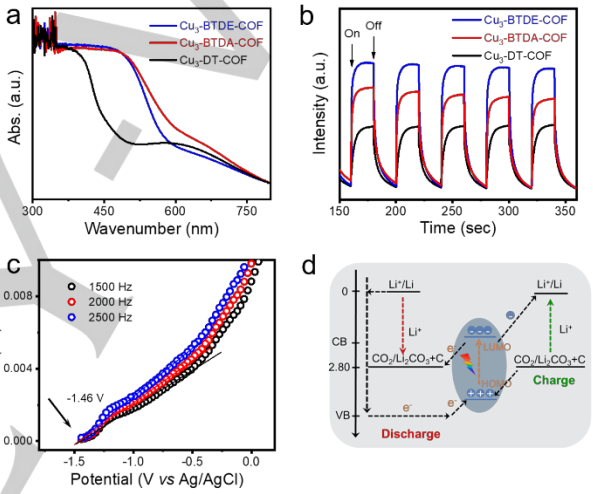

Figure 2. Characterizations of the optical properties for Cu_3-BTDE-COF, Cu_3-BTDA-COF and Cu_3-DT-COF. (a) UV-Vis absorption spectra. (b) Transient photocurrent response. (c) Mott-Schottky plots of Cu_3-BTDE-COF. (d) Energy diagram of Cu_3-BTDE-COF and standard potential of CO_2/Li_2CO_3 versus Li^+/Li.

Thus, Cu_3-BTDE-COF enables the sufficient utilization of photogenerated electrons/holes for CRR and CER. Moreover, we also have carried out the UV-Vis spectra and Mott-Schottky tests on Cu_3- BTDA-COF and Cu_3-DT-COF (Figure S16 and S17). According to the tests results, the conduction band potentials (1.49 V vs Li^+/Li) and valence band potentials (3.21 V and 4.01 V vs Li^+/Li) of Cu_3-BTDA-COF and Cu_3-DT-COF can also match with the redox potential (2.80 V vs Li^+/Li) of CO_2/Li_2CO_3. These results verify that both Cu_3-BTDA-COF and Cu_3-DT-COF can use light energy to complete the CRR and CER processes. In addition, the transient photocurrent response has been performed to study the charge transfer behaviors (Figure 2b). The intensity of transient photocurrent response for Cu_3-BTDE-COF is much higher than those of Cu_3-BTDA-COF and Cu_3-DT-COF (Figure 2b). Generally speaking, the enhancement of the photo-responsive of catalysts has a positive impact on their photocatalytic performance. Compared with Cu_3-BTDA-COF and Cu_3-DT-COF, Cu_3-BTDE-COF can theoretically generate more photoinduced electrons for CRR because of the specifical π-electron delocalization due to its sp^2 carbon linkage[50].

10.1002/anie.202402458

RESEARCH ARTICLE

In addition, we have carried out the electron paramagnetic resonance (EPR) tests to study its photogenerated electrons/holes transfer behavior. Under light conditions, the EPR signals of Cu_3-BTDE-COF, Cu_3-BTDA-COF and Cu_3-DT-COF are significantly higher than that under dark conditions at *g*=2.003 (Figure S18-S20). The result shows that the Cu_3-BTDE-COF, Cu_3-BTDA-COF and Cu_3-DT-COF can efficiently accelerate the electron-hole separation and prevent recombination [51]. Even though Cu_3-BTDE-COF, Cu_3-BTDA-COF, and Cu_3-DT-COF all have signals in the EPR tests. Furthermore, the intensity of EPR signals of Cu_3-BTDE-COF and Cu_3-BTDA-COF are stronger than that of Cu_3-DT-COF under the dark and light conditions at *g*=2.003 (Figure S19 and S20), which shows that thiazole is an important photosensitive group. The above results illustrate the photosensitivity of Cu_3-BTDE-COF, Cu_3-BTDA-COF and Cu_3-DT-COF, which may greatly benefit their application in light-assisted Li-CO_2 battery. Combining the ultraviolet photoelectron spectroscopy and Tauc curves, the LUMO and HOMO of Cu_3-BTDE-COF are calculated to be 1.84 V and 4.41 V vs. Li^+/Li, respectively (Figure S15). On account of the LUMO potential is lower than the reduction potential between CO_2 and Li_2CO_3/C (2.80 V vs. Li^+/Li), the photoelectrons can be applied in the discharge reactions of Li-CO_2 battery. Similarly, the holes can promote the charge reactions of Li-CO_2 battery in reverse charging process, because the HOMO is higher than the oxidation potential between Li_2CO_3/C and CO_2 (2.80 V vs. Li^+/Li). These results indicate that the efficient generation, separation, transfer, and utilization of photogenerated electrons and holes in the target cell process are promoted by the Cu_3-BTDE-COF photocathode.

Light-assisted Li-CO_2 battery. The electrochemical performances of Cu_3-BTDE-COF, Cu_3-BTDA-COF and Cu_3-DT-COF have been systematically evaluated as photocathodes of Li-CO_2 battery. Figure 3a, Figure S22 and S24 show the galvanostatic discharge/charge profiles of Li-CO_2 battery based on Cu_3-BTDE-COF, Cu_3-BTDA-COF and Cu_3-DT-COF photocathodes with/without illumination at 200 mA/g. The Cu_3-BTDE-COF photocathode under the dark condition displays discharge and charge voltages of 2.7 V and 4.1 V, respectively, with a lower round-trip efficiency of 65.8%. Under the light conditions, the discharge voltage of Cu_3-BTDE-COF photocathode increases to 3.32 V and the charging voltage decreases to 3.5 V, showing a high round-trip efficiency of 95.2%, indicating excellent light responsiveness of Cu_3-BTDE-COF photocathode (Figure 3a). In comparison, the discharge voltage and charge voltage of Cu_3-BTDA-COF photocathode under the dark conditions are 2.64 V and 4.2 V, respectively, corresponding to lower round-trip efficiency (62.85%). Under light conditions, the charge and discharge voltage are 3.65 V and 3.29 V, respectively, and the round-trip efficiency also increases to 90.13%. Cu_3-DT-COF presents the worst performance among them as a light-assisted Li-CO_2 battery under both dark (charge voltage, 4.31 V and discharge voltage, 2.56 V) and the light condition (charge voltage, 3.61 V and discharge voltage, 3.23 V). It has been reported that Cu_3 is a CO_2 reducing group, and Cu_3-DT-COF obtained through the covalent connection of Cu_3 and DT has faster charge transfer ability and higher absorbance compared with Cu_3[4]. Meanwhile, the energy round-trip efficiency of Cu_3-DT-COF under the light conditions is improved by about 30% compared to that under the dark conditions (Figure S21 and S22). Thus, Cu_3-BTDE-COF has the strongest response to light, compared to Cu_3-BTDA-COF and Cu_3-DT-COF, which may be due to the versatility produced by the many functional groups in Cu_3-BTDE-COF. After that, we have tested the rate capability at different current densities and the results showed that it could maintain low overpotentials at different current densities (Figure S23).

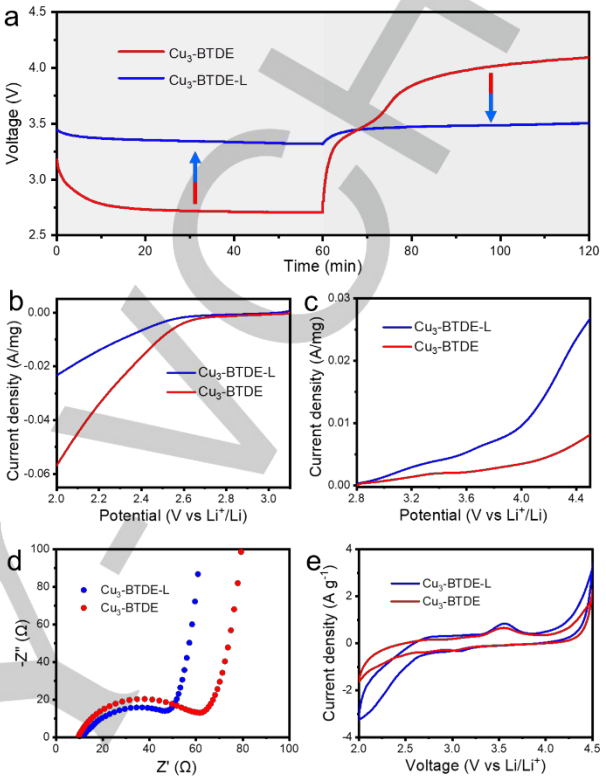

Figure 3. Battery performance of Cu_3-BTDE-COF. (a) Discharge and charge curves of the Cu_3-BTDE-COF based Li-CO_2 battery with and without illumination at 200 mA/g. (b) LSV curves of Cu_3-BTDE-COF cathode during CRR process. (c) LSV curves of Cu_3-BTDE-COF cathode during CER process. (d) EIS images of Cu_3-BTDE-COF with and without illumination at 200 mA/g. (e) CV curves of the Cu_3-BTDE-COF based cathode with and without illumination.

To gain insight into the influence of light on the Li-CO_2 battery, we have measured linear sweep voltammetry (LSV) curves in a CO_2-saturated 1.0 M LITFSI in tetraethylene glycol dimethyl ether (TEGDME) environment (Figure 3b and 3c). Under light conditions, the onset potentials and the limiting current density for the CRR and CER of Cu_3-BTDE-COF under light are much higher than those of Cu_3-BTDE-COF without light. The cyclic voltammetry (CV) results further confirm that the activity of the system has been improved with the assistance of light energy (Figure 3e). The performance test results of Li-CO_2 battery fully demonstrate their excellent properties. Thus, we have carried out cycling tests by Cu_3-BTDE-COF photocathode with and without illumination at 200 mA/g (Figure S24). These results indicate that the discharge and charging process of Cu_3-BTDE-COF in photo-assisted Li-CO_2 battery can be promoted by photogenerated electrons and holes, thus ensuring the cycling stability of Cu_3-BTDE-COF photoelectrode during the long-term cycling test. In addition, the theoretical thermodynamic potential of Li_2CO_3/C to CO_2/Li^+ is 2.80 V vs. Li^+/Li, meanwhile the value is 3.82 V vs. Li^+/Li for the self-decomposition of Li_2CO_3.[23] When the battery is cycled under light condition, the charging voltage is basically lower than 3.82 V, indicating that the charging process

10.1002/anie.202402458

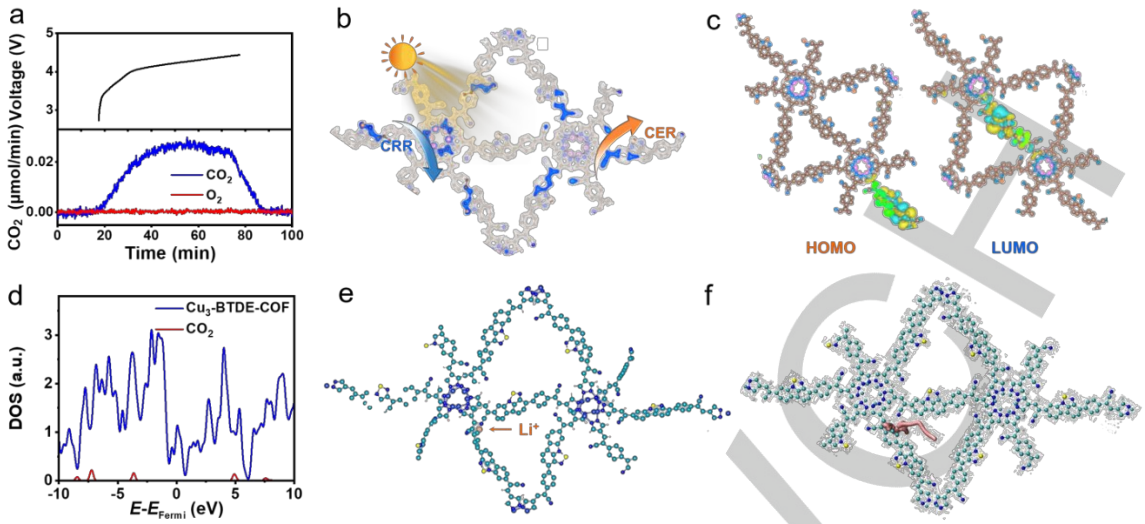

Figure 4. DFT calculations of Cu_3-BTDE-COF in light-assisted Li-CO_2 battery. (a) DEMS test during charging of the Li-CO_2 battery with Cu_3-BTDE-COF cathode catalyst. (b) Differential charge density diagram of Cu_3-BTDE-COF. (c) The associated HOMO and LUMO of Cu_3-BTDE-COF. (d) The density of states for Cu_3-BTDE-COF in light-assisted Li-CO_2 battery. (e) Theoretical calculation model of Li^+ with Cu_3-BTDE-COF. (f) The diffusion pathway for Li^+ to migrate on the structure model of Cu_3-BTDE-COF.

is more likely to be the co-decomposition of Li_2CO_3 and carbon species, rather than the self-decomposition of Li_2CO_3. During the operation of the battery, the inevitable accumulation of photocathode discharge products and the volatilization of liquid components in the electrolyte result in the decrease of cycle efficiency. In contrast, the batteries under dark condition are constantly subjected to severe polarization voltages, which can lead to adverse decomposition of battery materials or by-product formation [6, 24]. Afterwards, we have carried out the electrochemical impedance spectra (EIS) test to analyze the superior performance of Cu_3-BTDE-COF photocathode (Figure 3d). The semicircle of Cu_3-BTDE-COF under the light conditions is noticeably smaller than that of Cu_3-BTDE-COF under the dark conditions, proving the more excellent charge transfer kinetics of Cu_3-BTDE-COF in light-assisted Li-CO_2 battery [52]. These results have indicated that the introduction of light energy can indeed improve the charging and discharging performance of Li-CO_2 battery. We also conducted LSV and CV tests on Cu_3-BTDA-COF and Cu_3-DT-COF under light and dark conditions, respectively (Figure S25-S28), proving that Cu_3-BTDA-COF and Cu_3-DT-COF have stronger redox properties under light conditions.

Moreover, a series of tests have been conducted to study the by-products during the discharge/charge processes. Specifically, we have carried out the PXRD tests to determine the discharge products, and the main discharge products is Li_2CO_3 with or without light (Figure S29 and S30). However, it is clear from Figure S30 that Li_2CO_3 has lower crystallinity under light conditions, which means that the decomposition process becomes easier compared to dark conditions. In order to elucidate the work mechanism of light field and strong electric field on the battery reactions, the discharged/recharged Cu_3-BTDE-COF cathodes under the dark and light conditions were characterized. Then, we have performed SEM tests to study the different battery stages. From the SEM images, it can be seen that the morphology of the product is different under light and dark conditions. Under dark conditions, the detected discharge products are rod-shaped nanoparticles with sizes of ~1 μm) (Figure S31). Under light conditions, the morphology of the discharge products exhibits nanoflake morphology with a size of only ~100 nm, in significant contrast to that under dark condition (Figure S31). In order to further prove the complete reversibility of Cu_3-BTDE-COF photocathode of the battery, we have carried out in-situ differential electrochemical mass spectrometry (DEMS) test to evaluate the gas evolution during the charge process (Figure 4a). As shown in Figure 4a, DEMS testing can monitor the gas release of Cu_3-BTDE-COF cathode batteries during charging (Figure 4a), and only CO_2 gas has been detected. Based on the DEMS results, the charge to mass ratio (4.21 $e^-/3CO_2$) during the charging process can be determined, meaning that it basically matches with the reversible reaction of $4Li^+ + 3CO_2 + 4e^- \rightarrow 2Li_2CO_3 + C$. These results indicate that the battery performance can be effectively increased due to the synergistic effect of Cu_3-BTDE-COF photocathode catalyst.

Based on the above experiments results, theoretical calculations have been carried out to investigate the possible working mechanism of Cu_3-BTDE-COF photocathode in light-assisted Li-CO_2 battery. Initially, we have performed differential charge density test to analyze the charge distribution of Cu_3-BTDE-COF structure. As shown in Figure 4b, the interfacial charge density difference is depicted, in which the charge accumulation is presented as the blue region of Cu atoms on Cu_3, and the charge depletion is the gray region close to thiazole on BTDE (Figure 4b). This result shows that the electrostatic potential value around Cu_3 is positive, suggesting that it is more electrophilic than that of BTDE. Therefore, the result complies with above-mentioned experimental results that CRR and CER are more likely to locate in Cu_3 and BTDE, respectively (Figure 4b). To support this result, we have further conducted related calculations for the HOMO and LUMO distributions of Cu_3-BTDE-COF (Figure 4c, Figure S32 and S33). For Cu_3-BTDE-COF, its HOMO is mainly distributed on BTDE, while LUMO is mainly distributed on Cu_3 (Figure 4c). This also indicates that Cu_3 has a stronger affinity for electrons when compared with BTDE and Cu_3 and BTDE are the active centers of CRR and CER, respectively.

Afterwards, we have also conducted the calculations of density of states to demonstrate the relationship between CO_2 and Cu_3-BTDE-COF (Figure 4d and Figure S34). The calculation results show that the energy level of CO_2 is located within the band gap of Cu_3-BTDE-COF, thus there is a high possibility of electron transfer to CO_2. At the same time, it also verifies the good coupling between Cu_3-BTDE-COF and CO_2, which is much beneficial for CRR (Figure 4d) [6]. Then, theoretical calculations have been further performed to evaluate the possible interaction or diffusion effect of Li^+ (Figure 4e). Benefiting from the abundant functional groups in Cu_3-BTDE-COF, they would serve as hopping sites to be interacted with Li^+. We have calculated the possible adsorption site of Li^+ in Cu_3-BTDE-COF and the results show that Li^+ is more easily adsorbed near cyano group (Figure 4f). Beyond that, the Li^+ diffusion paths in the pore channels have also been calculated, and it tends to diffuse to the site of cyano group, supporting above-mentioned results (Figure 4f). Therefore, these results demonstrate the synergistic roles of Cu_3, BTDE and cyano group in promoting the electron-hole utilization, CO_2 adsorption/activation and Li^+ interaction/diffusion for Cu_3-BTDE-COF, which is much beneficial for the CRR and CER to largely improve the battery performance.

Conclusions

In summary, a series of MCOFs (i.e. Cu_3-BTDE-COF, Cu_3-BTDA-COF and Cu_3-DT-COF) with multiple active sites are synthesized by in-situ covalent connection of Cu_3 and BTDE, which can be utilized as efficient photocathode catalyst for light-assisted Li-CO_2 battery. Among them, Cu_3-BTDE-COF is a newly designed sp^2-carbon-linked based MCOF covalently linked by Cu_3 and thiazole-cyano group (BTDE), in which the existence of sp^2-carbon bond improves the stability of the skeleton and prolongs the π - electron conjugation time on the skeleton plane, meanwhile multiple active units (i.e., Cu cluster, thiazole and cyano sites) are beneficial to the CO_2 activation and evaluation processes. Specifically, Cu_3-BTDE-COF based battery delivers an ultra-low overpotential (0.18 V) and excellent round-trip efficiency (95.2%), outperforming the Schiff base COFs (i.e. Cu_3-BTDA-COF and Cu_3-DT-COF) and majority of the reported photocathode catalysts. Furthermore, theoretical calculations and characterization have shown that Cu_3-BTDE-COF with metal active centers, thiazole and cyano multifunctional groups possess strong CO_2 adsorption/activation and Li^+ interaction/diffusion ability to boost the CRR/CER kinetics and related battery efficiency. This work demonstrates the importance of sp^2-carbon-linked based MCOF by comparing the properties of Cu_3-BTDE-COF, Cu_3-BTDA-COF and Cu_3-DT-COF applied to light-assisted Li-CO_2 battery. It provides a reference for the application of different bonded COFs in light-assisted battery techniques.

Supplemental Information includes 34 figures, 5 tables.

Acknowledgements

This work was financially supported by the National Key R&D Program of China (2023YFA1507204), NSFC (Grants 22171139, 22225109, 22071109), Natural Science Foundation of Guangdong Province (no. 2023B1515020076), Postdoctoral Innovation Talent Support Program (BX20220116), Postgraduate Research & Practice Innovation Program of Jiangsu Province (KYCX23_1682).

Conflict of Interest

The authors declare no conflict of interest.

Keywords: Light-assisted CO_2 energy storage • Redox molecular junction • Photocatalysis • Metal-covalent organic frameworks

References

[1] a) N. Kittner, F. Lill, D. M. Kammen, *Nat. Energy* **2017**, *2*, 17125; b) Y. Li, A. Ozden, W. R. Leow, P. Ou, J. E. Huang, Y. Wang, K. Bertens, Y. Xu, Y. Liu, C. Roy, H. Jiang, D. Sinton, C. Li, E. H. Sargent, *Nat. Catal.* **2022**, *5*, 185-192; c) X.-X. Wang, X.-W. Chi, M.-L. Li, D.-H. Guan, C.-L. Miao, J.-J. Xu, *Chem* **2023**, *9*, 394-410; d) W. Zhang, F. Zhang, S. Liu, Wei K. Pang, Z. Lin, Z. Guo, L. Chai, *Proc. Natl. Acad. Sci.* **2023**, *120*, e2219692120.

[2] a) X. Xiao, Z. Zhang, P. Tan, *Proc. Natl. Acad. Sci.* **2023**, *120*, e2217454120; b) J.-H. Wang, S. Li, Y. Chen, L.-Z. Dong, M. Liu, J.-W. Shi, S.-L. Li, Y.-Q. Lan, *Adv. Funct. Mater.* **2022**, *32*, 2210259; c) S. Yang, P. He, H. Zhou, *Energy Environ. Sci.* **2016**, *9*, 1650-1654; d) Y. Qiao, J. Yi, S. Wu, Y. Liu, S. Yang, P. He, H. Zhou, *Joule* **2017**, *1*, 359-370. e) J. Zhou, T. Wang, L. Chen, L. Liao, Y. Wang, S. Xi, B. Chen, T. Lin, Q. Zhang, C. Ye, X. Zhou, Z. Guan, L. Zhai, Z. He, G. Wang, J. Wang, J. Yu, Y. Ma, P. Lu, Y. Xiong, S. Lu, Y. Chen, B. Wang, C.-S. Lee, J. Cheng, L. Gu, T. Zhao, Z. Fan, *Proc. Natl. Acad. Sci.* **2022**, *119*, e2204666119.

[3] a) Y. Zhang, R.-L. Zhong, M. Lu, J.-H. Wang, C. Jiang, G.-K. Gao, L.-Z. Dong, Y. Chen, S.-L. Li, Y.-Q. Lan, *ACS Central Sci.* **2021**, *7*, 175-182; b) Y. Qiao, J. Wu, J. Zhao, Q. Li, P. Zhang, C. Hao, X. Liu, S. Yang, Y. Liu, *Energy Storage Mater.* **2020**, *27*, 133-139; c) K. Wang, D. Liu, L. Liu, X. Li, H. Wu, Z. Sun, M. Li, A. S. Vasenko, S. Ding, F. Wang, C. Xiao, *Adv. Sci.* **2023**, *10*, 2205959.

[4] a) C. Yang, K. Guo, D. Yuan, J. Cheng, B. Wang, *J. Am. Chem. Soc.* **2020**, *142*, 6983-6990; b) S. Yang, Y. Qiao, P. He, Y. Liu, Z. Cheng, J.-j. Zhu, H. Zhou, *Energy Environ. Sci.* **2017**, *10*, 972-978; c) H. Gong, X. Yu, Y. Xu, B. Gao, H. Xue, X. Fan, H. Guo, T. Wang, J. He, *Inorg. Chem. Front.* **2022**, *9*, 1533-1540; d) J. Cheng, Y. Bai, Y. Lian, Y. Ma, Z. Yin, L. Wei, H. Sun, Y. Su, Y. Gu, P. Kuang, J. Zhong, Y. Peng, H. Wang, Z. Deng, *ACS Appl. Mater. Interfaces* **2022**, *14*, 18561-18569. e) X. Ma, W. Zhao, Q. Deng, X. Fu, L. Wu, W. Yan, Y. Yang, *J. Power Sources* **2022**, *535*, 231446.

[5] a) F. Ye, L. Gong, Y. Long, S. N. Talapaneni, L. Zhang, Y. Xiao, D. Liu, C. Hu, L. Dai, *Adv. Energy Mater.* **2021**, *11*, 2101390; b) B. Liu, Y. Sun, L. Liu, J. Chen, B. Yang, S. Xu, X. Yan, *Energy Environ. Sci.* **2019**, *12*, 887-922.

[6] a) L. Qie, Y. Lin, J. W. Connell, J. Xu, L. Dai, *Angew. Chem. Int. Ed.* **2017**, *56*, 6970-6974; b) Z. Zhang, Q. Zhang, Y. Chen, J. Bao, X. Zhou, Z. Xie, J. Wei, Z. Zhou, *J. Mater. Chem. A* **2015**, *54*, 6550-6553.

[7] a) X.-X. Wang, D.-H. Guan, F. Li, M.-L. Li, L.-J. Zheng, J.-J. Xu, *Adv. Mater.* **2022**, *34*, 2104792; b) K. Zhang, J. Li, W. Zhai, C. Li, Z. Zhu, X. Kang, M. Liao, L. Ye, T. Kong, C. Wang, Y. Zhao, P. Chen, Y. Gao, B. Wang, H. Peng, *Angew. Chem. Int. Ed.* **2022**, *61*, e202201718.

[8] a) D.-H. Guan, X.-X. Wang, F. Li, L.-J. Zheng, M.-L. Li, H.-F. Wang, J.-J. Xu, *ACS Nano* **2022**, *16*, 12364-12376; b) D.-H. Guan, X.-X. Wang, M.-L. Li, F. Li, L.-J. Zheng, X.-L. Huang, J.-J. Xu, *Angew. Chem. Int. Ed.* **2020**, *59*, 19518-19524; c) J. Li, K. Zhang, Y. Zhao, C. Wang, L. Wang, L. Wang, M. Liao, L. Ye, Y. Zhang, Y. Gao, B. Wang, H. Peng, *Angew. Chem. Int. Ed.* **2022**, *61*, e202114612.

[9] Z. Li, M.-L. Li, X.-X. Wang, D.-H. Guan, W.-Q. Liu, J.-J. Xu, *J. Mater. Chem. A* **2020**, *8*, 14799-14806.

[10] X.-X. Wang, D.-H. Guan, F. Li, M.-L. Li, L.-J. Zheng, J.-J. Xu, *Small* **2021**, *17*, 2100642.

[11] a) S. Zhao, C. Jiang, J. Fan, S. Hong, P. Mei, R. Yao, Y. Liu, S. Zhang, H. Li, H. Zhang, C. Sun, Z. Guo, P. Shao, Y. Zhu, J. Zhang, L. Guo, Y. Ma, J. Zhang, X. Feng, F. Wang, H. Wu, B. Wang, *Nat. Mater.* **2021**, *20*, 1551-1558; b) E. Jin, K. Geng, K. H. Lee, W. Jiang, J. Li, Q. Jiang, S. Irle, D. Jiang, *Angew. Chem. Int. Ed.* **2020**, *59*, 12162-12169; c) M. Leng, L. Fang, *Chem* **2022**, *8*, 2904-2906; d) Y.-L. Yang, Y.-R. Wang, L.-Z. Dong, Q. Li, L. Zhang, J. Zhou, S.-N. Sun, H.-M. Ding, Y. Chen, S.-L. Li, Y.-Q. Lan, *Adv. Mater.* **2022**, *34*, 2206706.

[12] a) H. aX. Li, C. Zhang, S. Cai, X. Lei, V. Altoe, F. Hong, J. J. Urban, J. Ciston, E. M. Chan, Y. Liu, *Nat. Commun.* **2018**, *9*, 2998; b) A. P. Côté, A. I. Benin, N. W. Ockwig, M. O'Keeffe, A. J. Matzger, O. M. Yaghi, *Science* **2005**, *310*, 1166-1170.

[13] a) J. Luo, X. Luo, M. Xie, H.-Z. Li, H. Duan, H.-G. Zhou, R.-J. Wei, G.-H. Ning, D. Li, *Nat. Commun.* **2022**, *13*, 7771; b) J.-N. Chang, Q. Li, Y. Yan, J.-W. Shi, J. Zhou, M. Lu, M. Zhang, H.-M. Ding, Y. Chen, S.-L. Li, Y.-Q. Lan, *Angew. Chem. Int. Ed.* **2022**, *61*, e202209289.

[14] a) E. Jin, M. Asada, Q. Xu, S. Dalapati, M. A. Addicoat, M. A. Brady, H. Xu, T. Nakamura, T. Heine, Q. Chen, D. Jiang, *Science* **2017**, *357*, 673-676; b) J. Xu, C. Yang, S. Bi, W. Wang, Y. He, D. Wu, Q. Liang, X. Wang, F. Zhang, *Angew. Chem. Int. Ed.* **2020**, *59*, 23845-23853; c) E. Jin, Z. Lan, Q. Jiang, K. Geng, G. Li, X. Wang, D. Jiang, *Chem* **2019**, *5*, 1632-1647.

[15] a) R.-J. Wei, P.-Y. You, H. Duan, M. Xie, R.-Q. Xia, X. Chen, X. Zhao, G.-H. Ning, A. I. Cooper, D. Li, *J. Am. Chem. Soc.* **2022**, *144*, 17487-17495; b) J. Dong, X. Han, Y. Liu, H. Li, Y. Cui, *Angew. Chem. Int. Ed.* **2020**, *59*, 13722-13733.

[16] a) Y. Kwon, J. Lee, Y. Noh, D. Kim, Y. Lee, C. Yu, J. C. Roldao, S. Feng, J. Gierschner, R. Wannemacher, M. S. Kwon, *Nat. Commun.* **2023**, *14*, 92; b) W. Wang, H. Zhang, S. Zhang, Y. Liu, G. Wang, C. Sun, H. Zhao, *Angew. Chem. Int. Ed.* **2019**, *58*, 16644-16650; c) X. Liu, P. Wang, H. Zhai, Q. Zhang, B. Huang, Z. Wang, Y. Liu, Y. Dai, X. Qin, X. Zhang, *Appl. Catal. B Environ.* **2018**, *232*, 521-530.

[17] a) J.-N. Chang, Q. Li, J.-W. Shi, M. Zhang, L. Zhang, S. Li, Y. Chen, S.-L. Li, Y.-Q. Lan, *Angew. Chem. Int. Ed.* **2023**, *62*, e202218868; b) H. Ding, Y.-R. Wang, M. Liu, J.-W. Shi, T.-Y. Yu, Y.-S. Xia, M. Lu, Y.-L. Yang, Y. Chen, S.-L. Li, Y.-Q. Lan, *Chem. Mater.* **2022**, *34*, 10752-10760.

[18] X. Liu, R. Qi, S. Li, W. Liu, Y. Yu, J. Wang, S. Wu, K. Ding, Y. Yu, *J. Am. Chem. Soc.* **2022**, *144*, 23396-23404.

[19] X. Li, J. Wang, F. Xue, Y. Wu, H. Xu, T. Yi, Q. Li, *Angew. Chem. Int. Ed.* **2021**, *60*, 2534-2540.

[20] G. Liu, G. Zhao, W. Zhou, Y. Liu, H. Pang, H. Zhang, D. Hao, X. Meng, P. Li, T. Kako, J. Ye, *Adv. Funct. Mater.* **2016**, *26*, 6822-6829.

[21] a) J. Liu, Y. Liu, N. Liu, Y. Han, X. Zhang, H. Huang, Y. Lifshitz, S.-T. Lee, J. Zhong, Z. Kang, *Science* **2015**, *347*, 970-974. b) Y. Wang, J. Zhou, C. Lin, B. Chen, Z. Guan, A. M. Ebrahim, G. Qian, C. Ye, L. Chen, Y. Ge, Q. Yun, X. Wang, X. Zhou, G. Wang, K. Li, P. Lu, Y. Ma, Y. Xiong, T. Wang, L. Zheng, S. Chu, Y. Chen, B. Wang, C.-S. Lee, Y. Liu, Q. Zhang, Z. Fan, *Adv. Funct. Mater.* **2022**, *32*, 2202737.

[22] a) H. Liu, D. Wang, Z. Yu, Y. Chen, X. Li, R. Zhang, X. Chen, L. Wu, N. Ding, Y. Wang, Y. Zhao, *Sci. China Mater.* **2023**; b) X.-F. Qiu, J.-R. Huang, C. Yu, Z.-H. Zhao, H.-L. Zhu, Z. Ke, P.-Q. Liao, X.-M. Chen, *Angew. Chem. Int. Ed.* **2022**, *61*, e202206470.

[23] C. Wu, Z. Teng, C. Yang, F. Chen, H. B. Yang, L. Wang, H. Xu, B. Liu, G. Zheng, Q. Han, *Adv. Mater.* **2022**, *34*, 2110266.

[24] Y.-R. Wang, H.-M. Ding, X.-Y. Ma, M. Liu, Y.-L. Yang, Y. Chen, S.-L. Li, Y.-Q. Lan, *Angew. Chem. Int. Ed.* **2022**, *61*, e202114648.

10.1002/anie.202402458

Entry for the Table of Contents

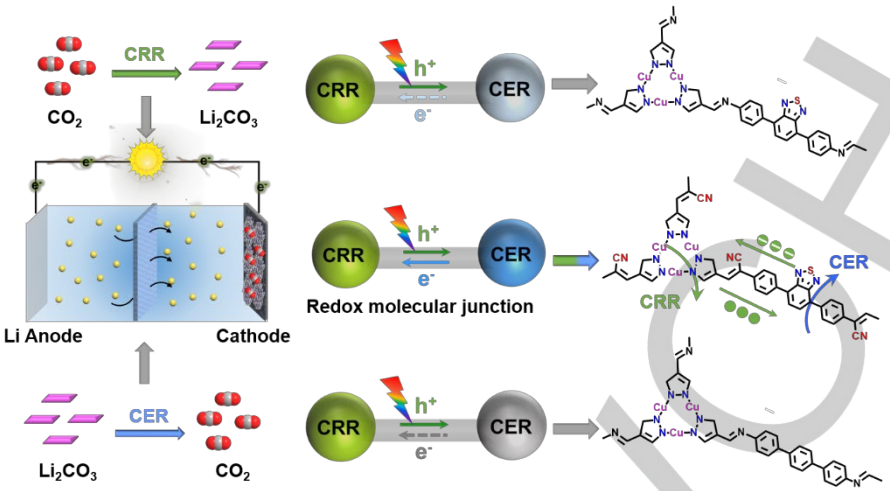

A kind of redox molecular junction sp^2 carbon-conjugated metal-covalent organic framework with multiple active sites have been prepared and can be successfully applied for light-assisted CO_2 energy storage.